Finite element analysis of the effect of porosity on residual stress in 2024 aluminium alloy GTAW

Materials Research Express

PAPER

Finite element analysis of the effect of porosity on residual stress in 2024 aluminium alloy GTAW

Pattarawadee Poolperm[1,2], **Wasawat Nakkiew**[2,3,5] **and Nirut Naksuk**[4]

[1] Graduate Program in Industrial Engineering, Department of Industrial Engineering, Faculty of Engineering, Chiang Mai University, Chiang Mai, Thailand
[2] Advanced Manufacturing Technology Research Center (AMTech), Department of Industrial Engineering, Faculty of Engineering, Chiang Mai University, Chiang Mai 50200, Thailand
[3] Department of Industrial Engineering, Faculty of Engineering, Chiang Mai University, Chiang Mai, Thailand
[4] Automation for Material Processing Research Team, Material Processing and Manufacturing Automation Research Group at the National Metal and Materials Technology Center (MTEC), National Science and Technology Development Agency (NSTDA), Thailand Science Park, Pathum Thani, Thailand
[5] Author to whom any correspondence should be addressed.

E-mail: pattarawadee_pool@cmu.ac.th, wasawat@eng.cmu.ac.th and nirutn@mtec.or.th

Keywords: finite element analysis, gas tungsten arc welding, porosity, 2024 aluminium alloy, double-ellipsoid heat source, residual stress

OPEN ACCESS

RECEIVED
2 April 2020

REVISED
25 April 2020

ACCEPTED FOR PUBLICATION
5 May 2020

PUBLISHED
13 May 2020

Abstract

Simulations of the welding process for butt joints using finite element analysis (FEA) of the effect of porosity are presented. The metal used was aluminium alloy (grade 2024), and the filler material was alloy ER5356. The simulations were performed using the commercial software ANSYS, considering a double ellipsoid heat source, temperature-dependent material properties, material deposits, mechanical analysis, transient heat transfer, and defects (porosity). In this study, the FEA simulations were constructed for two types of heat source (single- and double-ellipsoid) used in gas tungsten arc welding (GTAW), and the calculated residual stress results were compared with the experimental values. Two double ellipsoid models were constructed for cases with and without porosity. The porosity was measured by three-dimensional (3D) computed tomography (CT), and the size and location of pores were mapped onto the weld bead created by the birth-and-death technique.

1. Introductions

Aluminium alloys (2xxx and 7xxx series) are mostly used to produce aerospace components with high specific strength [1, 2] and high-strength precipitation hardening. The 2024 aluminium alloy is typically employed in automobile, aerospace, and radar fields because of its high strength, low density, and excellent heat resistance [3, 4]. For instance, it may be used to make the skin, frames, panels, piston, blades, cylinder head, and screws during the production of aircraft and liquid-fuel tanks of rockets.

Gas tungsten arc welding (GTAW), which is distinguished by high controllability and low cost of equipment, is widely used for sheet precision welding. It is also known as tungsten inert gas (TIG) and is a well-known welding technique for a wide range of materials [5]. Gas tungsten arc welding uses a non-consumed tungsten electrode with inert gas, such as argon, as a shielding gas [6]. Thus, the arc welding of aluminium alloy is of great importance in producing high-strength alloy, which leads to lighter and cheaper structures [7].

One of the major problems associated with the welding of aluminium alloys is the formation of gas porosity [8]. Porosity is an important factor responsible for the degradation of mechanical properties. Large porosity affects the mechanical properties of welded joints. It is essential to identify the cause of porosity formation to prevent its occurrence. The major reason for the formation of pores is hydrogen. Hydrogen present in the weld metal or arc atmosphere is often the root cause of the formation of a variety of defects, but also an important reason for the reduction in the mechanical properties of the weld metal. Hydrogen is the only gas in molten aluminum which has significant solubility. The welded pool will absorb and dissolve hydrogen during the welding of aluminum alloy in proportion to its partial pressure in the arc atmosphere. The solubility of hydrogen in the molten aluminum is about 20 times higher than that in the solid aluminum. Thus, once hydrogen has

Table 1. The welding experimental conditions of 8 welding specimens.

No.	Arc current (A)	Welding speed (mm min^{-1})	Wire feed rate (mm min^{-1})
1	180	240	700
2	180	240	400
3	180	210	700
4	180	210	400
5	130	240	700
6	130	240	400
7	130	210	700
8	130	210	400

been introduced into the weld pool in welding, weld porosities would form while the weld pool containing dissolved gases above the solubility limit in solid aluminium [8].

After welding, the current detection of internal porosity is often achieved using an x-ray process, which is also used offline. The high cost of welding quality inspection has become a bottleneck restricting the development of high-efficiency welding technology. In this research, porosities were analyzed by preliminary radiographic test (RT) and three-dimensional (3D) computed tomography (CT). In the simulation of pores characteristics, the size and position of the pores were obtained from RT and CT and then used to create a CAD model that is closest to reality as possible. There are 8 actual workpieces of welded. The workpiece has the most size and pores distribution characteristics (sample number 7), which will be simulated in this step by using the SOLIDWORKS program. FEA was implemented by creating a simulation of GTAW and pores characteristics occurring by using ANSYS Software. In the analysis of the distribution of residual stress in the welds, the porosities effect that affects the residual stress in the welds from the GTAW, an element type of SOLID 90, which is a single degree of independence, as the heat-based element is used for this analysis. By determining the thermal and mechanical properties of aluminum alloy grade 2024 as shown in table 1. Since each temperature is not stable, the properties of each temperature are not equal. The simulation, therefore, requires different thermal and mechanical properties at different temperatures.

Residual stresses occur throughout the area of solidified weld metal, and the heat-affected zone (HAZ) in a welded joint [9] and distortion in welding are primarily caused by the transient thermal cycles in the vicinity of the weld [7]. Due to the high intensity of the localised heat source, a non-uniform transient temperature field occurs. Many techniques have been used to measure residual stress in aluminium alloy, including the hole-drilling method [10], the x-ray diffraction (XRD) method [11, 12], and the holographic interferometry method [13], just to name the most popular. In this research, XRD, which is typically used to measure residual stress [14], was used to measure residual stress in longitudinal and transverse directions.

Many researchers have studied the prediction of welding residual stresses. Finite element analysis (FEA) has been utilised by several authors to perform welding simulation and to forecast welded residual stress in different types of joints and materials [15–17]. A finite element simulation is an essential tool for accurately predicting welding distortion and residual stresses in welded structures [9]. Fricke *et al* [18] used the full 3D pipe welding model and presented residual stress on two different diameters of the pipe. Oddy *et al* [19] reported that the prediction of the temperature field requires a nonlinear transient 3D analysis. The consequences of some welding parameters on residual stresses [15] have been studied by Ribycki *et al* [20], who investigated the effect of wall thickness and pipe diameter using the axisymmetric FEA model with lateral symmetry for multi-pass welding of stainless steel pipes. In weld simulation, computational software on an FEA program such as ANSYS, ABAQUS, MSC/MARC, and SYSWELD are popular [21, 22]. The FEA package ANSYS is used in this research. It is one of the most efficient pieces of finite element (FE) calculation software and is used to evaluate residual stress, the effect of porosity, and the analysis of basic structural and heat-transfer problems. Zubairuddin *et al* [21] used SYSWELD software for the thermo-mechanical analysis and created a 3D meshed model for the simulation and used a double ellipsoidal heat source distribution for the thermal analysis. Klobčar *et al* [23] used ABAQUS computer for finite element modeling of the GTA weld-surfacing process. The model developed was applied to predict deformation and residual stresses, and to detect areas critical to cracking when complex-geometry tooling was repaired. Moreover, Na *et al* [3] studied metals heat-treated under high pressure on 2024 aluminium alloy while restricting expansion-deformation heat-treatment by using the ABAQUS finite element software, and the effects of the mould material properties.

From the foregoing, it was found that the creation of a three-dimensional finite element model on the analysis of pore sizes and distributions did not produce much research. Besides, Wei [24] used a linear discriminant analysis (LDA) prediction rule for weld surface porosity in gas metal arc welding (GMAW) based

Figure 1. Butt-joint welded specimen.

on a statistical analysis of arc current. Therefore, recent work has led to the development of such a model, for the prediction of residual stress, size, and distribution of pores in the bead on plate welds in 2024 aluminium alloy. Process modeling and experimentation are both used to address the key problems in the retention of good post-weld microstructures and properties and the control of residual stress and distortion for welding of 2024 aluminium alloy or other materials.

The objective of this research was to investigate the possibility of 'pores' in a corresponding 3D finite element model with the XRD method for the purpose of calculating the magnitude and distribution of the welding residual stresses. In this work, first, a comparison between the single heat source model and the double-ellipsoid heat source model by FEA and XRD was conducted. Then, a comparison of the results of the FEA with porosity, FEA without porosity, and actual XRD results was carried out. To create a finite element model, the porosity in GTAW, pore shape, and pore distribution were entered into the FEA program from 3D with computed tomography and SolidWorks programs [25]. To this end, 3D FEA based on statistical analysis and a prediction model for porosity defects was developed and verified under welding conditions. Therefore, the models mimicked a real welding situation where porosity occurs in the weld bead.

2. Material and welding procedure

To achieve maximum efficiency from the test, the experimental design or research method design is needed by using scientific processes. The welding conditions are defined by the full factorial design method. From the literature review that studied the welding of aluminum alloy by GTAW, it's found that the factors may affect the size, the characteristics of the porous distribution and the residual stress values occur, all 3 factors including (1) arc current, (2) welding speed and (3) wire feed rate. In this research, each factor has 2 levels which are high level and low level. The welding experimental conditions of 8 welding specimens as shown in table 1. It is reliable to predict the residual of other welding conditions based on the given welding conditions. In the simulation of pores characteristics, the size and position of the pores were obtained from RT and CT. The RT found that sample number 7 had in the most pores. With budget constraints, the measurement of the work is quite high and expensive, therefore we will choose only the most pores workpiece to measure in CT (3D).

As for FEA, the purpose of predicting residual stress in the present welds, FE analysis is essential to capture sufficient detail in the thermal field. It is, however, important to optimise the complexity of the FE implementation to achieve acceptable accuracy efficiently, particularly for transient thermal problems such as the present case which are far from steady-state conditions. Validation against experimental results is conducted on the basis of residual elastic strain, rather than stress, since it is strain that is actually measured. Difficulties, however, include the avoidance of hot cracking during welding, the development of good post-weld microstructures and properties, and the control of residual stress and distortion.

Gas tungsten arc welding is widely used for welding aluminium, and it produces welds of good appearance and quality [1]. The square butt joint configuration shown in figures 1 and 2 was prepared to fabricate GTAW joints. The plates of 2024 aluminium alloy were cut into the required size: 150 $\times$ 100 $\times$ 3.2 mm (width $\times$ length $\times$ thickness). A welding arc was initiated between the tungsten electrode and the aluminium alloy specimen. An alternating current and high frequency (ACHF) method [26] was used because it generally helps reduce the chance of oxide film formation on the surface of welded areas.

The GTAW was performed on a welding machine of model 275 Precision TIG from Lincoln Electric Company. Further, ER5356 (1.2 mm diameter) wire was used during the welding process as a filler material. The aluminium alloy grade 2024 had the following welding conditions: gas flow rate 8 l min^{-1}, arc gap 3 mm, welding angle 90 degrees, and welding frequency 20 Hz. The weld was made in a straight direction and with full

Figure 2. The joint prepared prior to welding.

Table 2. Properties of 2024 aluminium alloy [3].

Temp (C)	Thermal conductivity ($W.m^{-1}\ K^{-1}$)	Specific heat capacity (KJ/kg.C)	Elastic modulus (GPa)	Poisson's ration	Yield strength (MPa)	Density ($kg\,m^{-3}$)	Thermal expansion coefficient (10^{-6})
20	164	881	72.4	0.33	473.0	2780	14.000
100	182	927	66.5	0.33	416.5	2780	23.018
200	194	1047	63.5	0.33	293.5	2780	24.509
300	202	1130	60.4	0.33	239.8	2780	25.119
400	210	1210	56.1	0.33	150.0	2780	25.594
500	220	1300	50.0	0.33	100.0	2780	26.637

penetration. The weld pass is a single-pass GTAW. The temperatures of the aluminium alloy are shown in table 2. The butt-joint welded specimen and the joint prepared prior to welding are shown in figures 1 and 2.

3. Governing equations

Based on the above assumptions, the conservation equations can be written. The heat transfer equation in a stationary orthogonal curvilinear coordinate system (x, y, z) [17] that depends on the time of the formation of solids in 3D is expressed as follows:

$$\frac{\partial}{\partial x_i}\left(k_{x_i}\frac{\partial T}{\partial x_i}\right) + Q = \rho c\frac{\partial T}{\partial t} \tag{1}$$

where ρ represents the mass density, c represents the specific heat capacity, k_{x_i} represents the tensor of the coefficient of thermal conductivity, Q represents the heat input, T constitutes the temperature variation as a function of distance in the axis x_i, and time t, and x_i represents the main axial distance [17]. The stress equation is written as

$$\sigma_{ij} = \lambda\delta_{ij}e + 2G\varepsilon_{ij} - (3\lambda + 2G)\delta_{ij}\alpha(T - T_0) \tag{2}$$

where σ_{ij} is the stress tensor, T_0 is the reference temperature at zero stress, α is the expansion coefficient, ε_{ij} is the strain tensor, and δ_{ij} is equal to 1 when $i = j$ or $i \neq j$.

$$\lambda = \frac{\nu E}{(1+\nu)(1-2\nu)},\ G = \frac{E}{2(1+\nu)},\ e = \varepsilon_{11} + \varepsilon_{22} + \varepsilon_{33} \tag{3}$$

where ν is the Poisson's ratio, and E is the modulus of elasticity.

According to the double-ellipsoid heat source model, the heat source was divided into front and rear sections, each of which had a separate distribution of heat flux. A volumetric heat flux model proposed by Goldak is implemented in the model [27]. The volumetric heat flux in the front and rear regions is defined as follows in equations (4) and (5) [27–30]

For the front heat source,

$$q(x, y, z) = \frac{6\sqrt{3}f_f\eta VI}{abc_f\pi\sqrt{\pi}}e^{-3x^2/a^2}e^{-3y^2/b_f^2}e^{-3z^2/c^2} \tag{4}$$

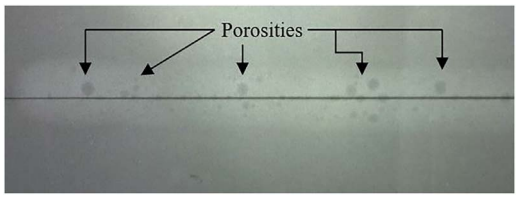

Figure 3. Example of a radiographic test (RT) film. (When passing through the film washing process, it appears as dark spots or dark-round [porosities]).

Table 3. Chemical composition (wt %) of 2024 aluminium alloy [14, 33].

Cr	Cu	Fe	Mg	Mn
⩽0.10	3.80–4.90	⩽0.50	1.20–1.80	0.30–0.90
Si	Ti	Zn	Other	Al
⩽0.50	⩽0.15	⩽0.25	⩽0.15	Bal.

and for the rear heat source,

$$q(x, y, z) = \frac{6\sqrt{3} f_r \eta V I}{abc_r \pi \sqrt{\pi}} e^{-3x^2/a^2} e^{-3y^2/b_f^2} e^{-3z^2/c^2} \tag{5}$$

where v is the voltage during welding, I is the arc current, and η is the arc efficiency with $b_f = a$, $b_r = 4b_f$, and $f_f + f_r = 2$; b_f is the distance of the front heat flux, b_r is the distance of the rear heat flux [27]. The geometric parameter a, b_f, b_r and c are schematically shown in figure 3. The relationship between these heat-deposited fractions and geometric parameters is as below [31]:

$$f_f = \frac{2b_f}{(b_f + b_r)} \tag{6}$$

$$f_f = \frac{2b_r}{(b_f + b_r)} \tag{7}$$

The front half of the source is the quadrant of one ellipsoidal source and the rear half is the quadrant of another ellipsoid, and this figure also shows the distribution of power density along the y-axis [27, 32, 33].

In the model, the sample material is 2024 aluminium alloy, and the square butt-joint welded specimens. The properties and chemical composition are shown in tables 2 and 3, [3] respectively. The analysis of the chemical composition was performed by using energy dispersive x-ray fluorescence (EDXRF).

4. X-ray computed tomography (CT)

During the welding process, pores (also known as cavity pockets) frequently occur and are the characteristic feature of aluminium alloy welding. This is usually done offline. Nevertheless, the x-ray technique cannot separate the overlapping porosities in the thickness direction [8]. After welding, the pores are frequently inspected by x-ray. Monitoring technology based on the use of radiographic tests [31], ultrasound [34], infrared thermography [35], and image processing [36] have been proposed.

The inspection of the porosity and its size of all 8 welding specimens were measured. In this research, the RT was an x-ray YXLON machine series YSMART583 [26]. An example of RT film from sample number 7 is shown in figure 3, where all the black dots are pores. The results showed that the number of pores $\times$ average size of the pore at the arc current of 130 A, welding speed of 210 mm min^{-1}, and wire feed rate of 700 mm min^{-1} (sample number 7) resulted in the most pores.

After that, the porosity was detected, and its size was measured by 3D x-ray CT to lower the cost of inspecting defective welds in 3D, which are quite expensive. Therefore, researchers will select only the most porous specimens to detect defects in three dimensions. Sample number 7 was chosen to measure the three-dimensional pores to achieve more precision using 3D x-ray CT. X-ray CT with cone-beam geometry has been used for non-destructive characterization and evaluation of materials [37]. X-ray transmission investigated the specimen using the same type of x-ray tube as in the micro-focused x-ray transmission imaging system [8]. Computed tomography has become an essential and effective method in the analysis of the internal structure of

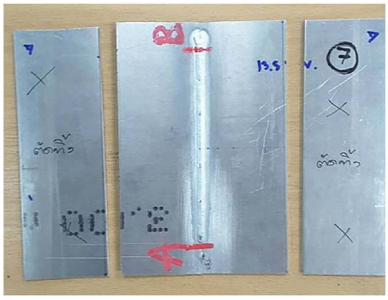

Figure 4. Size and characteristic of the measured specimen by 3D x-ray CT.

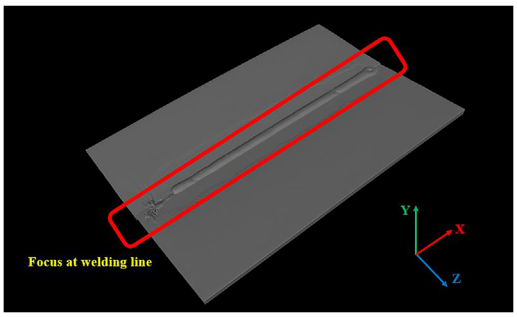

Figure 5. Welding line.

Table 4. Scanning parameters.

Parameters	Details
System	GE Phoenix V V|tome|x S 240KV
ACQ/REC. software	Datos|x 2.2
Tube voltage	175 kV
Tube current/Target power	600 μA/105 W
No. of images	1500
Voxel size	100
Total scan time	33 min
Filter	1 min Sn
Reconstruction time	<2 min
Analysis software	VG Studio Max 3.0

materials, allowing pores, cracks, or defects to be visualised and evaluated in the materials [38, 39]. Therefore, 3D x-ray CT was used. The shape, size, porosity, and quantity of pores formed during aluminium alloy welding were determined by 3D x-ray computerised axial tomography. The longitudinal section and cross-section of weld beads were polished and etched. In addition, the shapes of pores were observed. The size and characteristics of the measured specimen are shown in figure 4.

The CT system could not separate a defect smaller than 70 μm in the analyzed specimens [38]. The scanning parameters are shown in table 4.

The CT images (figures 5, 6) show that the porosity is dense near the center of the welding line. Computed tomography can clearly specify the location of the pores. In addition, it can measure pores with overlapping characteristics along the weld as well as the size of pores in 2024 aluminium alloy. The summary of the porosity analysis of the samples using the CT method is shown in table 5. Preliminary observation from both CT image and residual stress results suggested that the area with high porosity was likely to create tensile residual stress on the surface [8], which could decrease the surface integrity and strength of the material. Top and side view cross-section of 2024 aluminium alloy as shown in figures 7, 8.

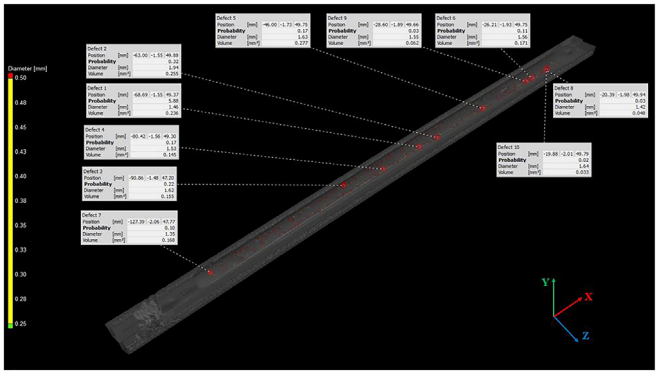

Figure 6. Top 10-point biggest diameter.

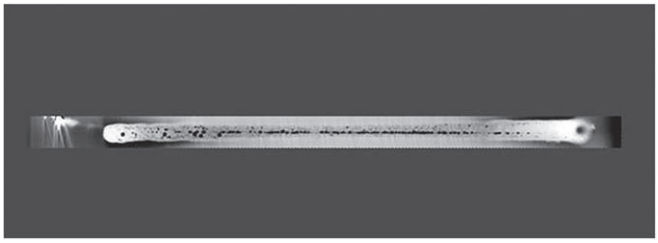

Figure 7. Top view cross-section of 2024 aluminium alloy.

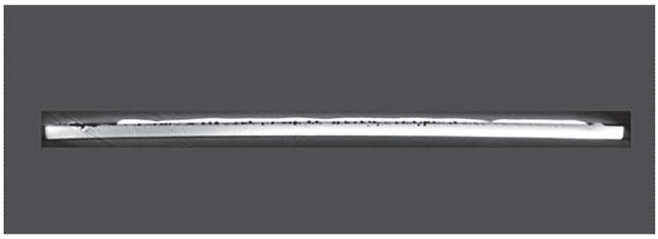

Figure 8. Side view cross-section of 2024 aluminium alloy.

Table 5. The number of pores (defects) detected with 3D computed tomography (CT).

Diameter (mm)	Number of pores (N)	Average pore size (mm)
<0.15	158	
0.15–0.30	55	
0.30–0.45	110	
0.45–0.60	84	
0.60–0.75	42	0.4549
0.75–0.90	47	
0.90–1.05	38	
>1.05	26	
Total	560	

From the measurement of the pore quantity of 2024 aluminium alloy by RT method, it was found that the pore volume can be measured in 2D form, which cannot directly determine the pore volume. In here, it assumes the appearance of pore characteristic of all sphere, but in fact, the pores perhaps not spherical, it may be a

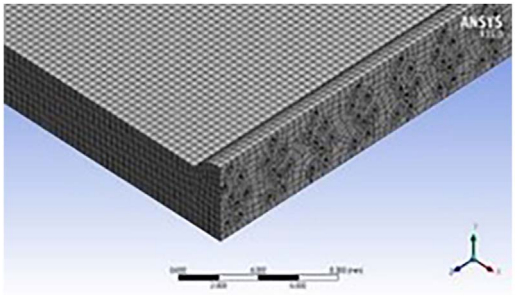

Figure 9. Cross-section of the welding specimen internal porosity and mesh sizing.

distorted shape from the sphere resulting in various values including the residual stress value that occurs maybe slightly distort. At the same time, the porosity of 2024 aluminum alloy was measured by the CT method, it can be measured in 3D which can indicate the volume of all pores along the weld (the characteristics of overlapping pores). This is consistent with the appearance of actual pores, resulting in the residual stress values that occur match reality.

5. FEA model (simulation)

A finite element model for predicting the evolution of stress and distortion for a bead on the plate of GTAW in the 2024 aluminium alloy plate has been described [7]. The FEA model consisted of sequential uncoupled thermal and mechanical analysis. According to Mousavi and Miresmaeili [40], Ueda and Yamakawa in 1971 used 2D finite element analysis to calculate the welding residual stresses for the first time, and McDill *et al* in 1990 were the first to perform 3D analyses to predict residual stresses in the large welds [5, 40]. The effect of geometry configuration on residual stress was analyzed and compared with findings from the x-ray diffraction method. Many other FEA models have also been suggested to estimate residual stresses. Deng and Murakawa [41] developed a 3D FEA model that simulates residual stresses during a pipe's multipass weld. Owen *et al* [42] provided comparisons with residual stress developed during welding of aluminium alloy AA2024 among neutron diffraction, x-ray diffraction, synchrotron x-ray diffraction, and finite element model results.

In this research, the FEA method was used to model gas tungsten arc welding with porosity. The finite element model was constructed using ANSYS simulation software. Further-more, the ANSYS program predicts residual stress from butt-joint welding by gas tungsten arc welding of 2024 aluminium alloy. The aerospace industry uses 2024 aluminium alloy in many aircraft parts and spacecraft components. The specimen dimension was 150 $\times$ 100 mm with a thickness of 3.2 mm. This finite element analysis model used a SOLID 90 element for welding analysis [43] and was constructed from a double-ellipsoid heat source on the same surface. Then, heat flux was moved from the surface of one element onto the next element until the welding process was complete using the birth and death technique [44]. Porous simulation in welding can only assume that the reduction in a cross-sectional area associated with porosity is what affects residual stress. Finite element methods are essential in order to capture the coupling between thermal histories, elastic properties at high temperatures, and residual stress of the consequent development [14]. In this article, the model is adapted to the more practical situation of a square butt weld. Detailed validation is a key aspect of the construction of any reliable process model. The cross-section of the welding specimen's internal porosity and mesh sizing is shown in figure 9.

The comparison of the finite element model is presented below.

1. XRD measurement of 304 stainless steel, 304 stainless steel (single heat source) and 304 stainless steel (double-ellipsoid heat source) models:
   We compared the differences in the residual stress values between all three methods. The longitudinal residual stress results of references [22, 44] and GTAW of 304 stainless steel (size of 150 $\times$ 100 mm and thickness of 0.3 mm) with a single heat source and residual stress from the XRD measurements of the actual welding are shown in table 7. A comparison of longitudinal residual stress results between the XRD measurement, single heat source, and double-ellipsoid heat source of 304 stainless steel is shown in table 5.
2. Model of 2024 aluminium alloy with porosity and without porosity (double-ellipsoid heat source):

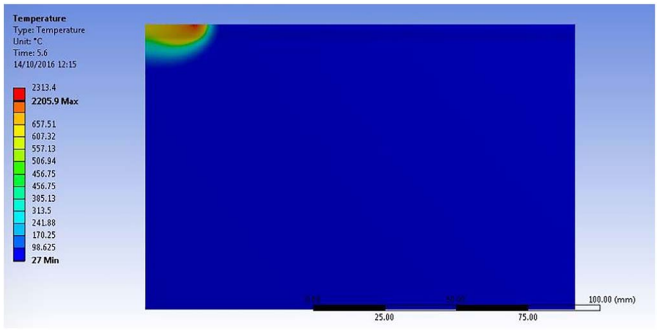

Figure 10. Welding simulation with birth–death technique of 304 stainless steel (double-ellipsoid heat source).

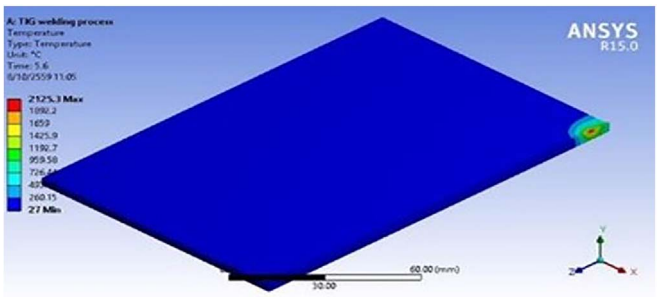

Figure 11. Welding simulation with birth–death technique of 2024 aluminium alloy without porosity (double-ellipsoid heat source).

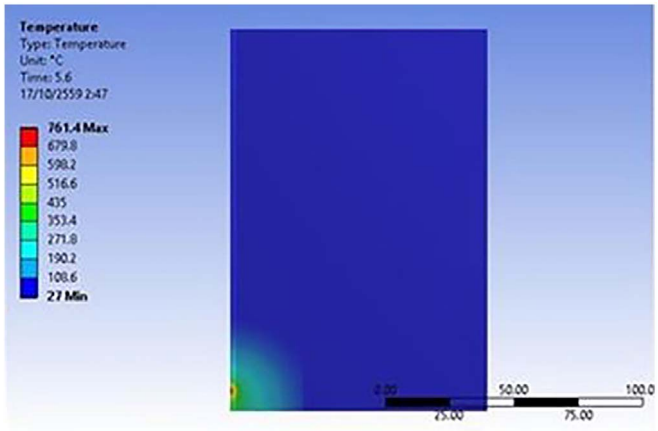

Figure 12. Welding simulation with the birth–death technique of 2024 aluminium alloy with porosity (double-ellipsoid heat source).

The model used 3,391,078 nodes and 773,500 elements. Moreover, the 2024 aluminium alloy model has a mesh size of 0.4 × 0.4 mm, and the porosity mesh size is 0.05 mm. Results of the FEA model of 304 stainless steel (double-ellipsoid heat source), FEA model of 2024 aluminium alloy without porosity and porosity (double-ellipsoid heat source) are shown in figures 10–12.

After simulating welding and cool down until the temperature of the specimen was equal to room temperature with transient thermal analysis, the program analysis was changed from transient thermal analysis to static structural analysis to investigate residual stresses. A comparison of longitudinal residual stress results between the XRD measurement, welding simulation without porosity, and welding simulation with porosity of the double-ellipsoid heat source of 304 stainless steel is shown in table 6.

Figure 13. Stresstech x-ray diffraction (XRD) machine.

Table 6. Comparison of longitudinal residual stress results in 304 stainless steel from XRD, single heat source, and double-ellipsoid heat source.

Distance from the weld center (mm)	5	10	20	30	40
Residual stress from XRD [22, 44] (MPa)	186.9 ±20.2	−299.6 ±26.1	−204.0 ±37.0	−180.1 ±46.1	−157.2 ±55.4
Residual stress from FEA, 304 stainless steel (single heat source) [22, 44] (MPa)	201.59	−287.24	−263.05	−238.37	−212.67
Residual stress from FEA, 304 stainless steel (double-ellipsoid heat source) (MPa)	165.10	−290.91	−214.50	−186.90	−172.59

6. Residual stress measurement

Residual stresses in a body are those that are not required to maintain equilibrium between the body and its environment [11]. Residual stresses have been measured in the GTAW butt-joint welded 2024 aluminium alloy plate using synchrotron XRD.

In this research, welding conditions were generated by the use of a full factorial experimental design technique. The variables used were arc current, welding speed, and wire feeding rate [44]. The residual stress measurement of sample number 7, which produces the most porosity, was performed with a Stresstech x-ray diffraction machine (X-STRESS 3000) [26, 44], which uses a copper-containing x-ray tube. The machine is equipped with a Cr x-ray tube source radiation of wavelength $\lambda = 2.084\ 87$ Å. Baisukhan *et al* [22] used XRD to measure non-destructively and predict residual stresses in the large welds for GTAW. The ψ-angles (0, ±18.4°, ±26.6°, ±33.2°, ±39.2°, ±45°) were used. The XRD method, known as the sin2ψ method [45], was used to measure the RS. The X-STRESS 3000 is shown in figure 13.

The welding positions were measured with x-ray diffraction and finite element model in the center of the weld zone (the liquid region where the process itself takes place and is adjoined by the fusion boundary), at the following distances from the welding line: 0, 5, 10, 20, 30, and 40 mm, as shown in figure 14. The residual stress was measured in the longitudinal direction (along the center line-H direction) and in the transverse direction.

7. Results

In table 6, the distance from the center of the weld at 5 mm is near the welding line, which is the area of the heat-affected zone (HAZ). There is a very high temperature, but the temperature is not high enough to melt into the

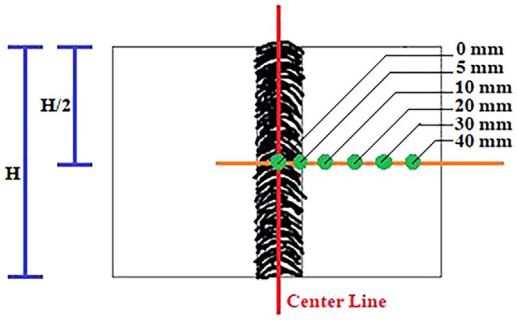

Figure 14. The location used to measure (by finite element analysis (FEA) and XRD) the residual stress of welding.

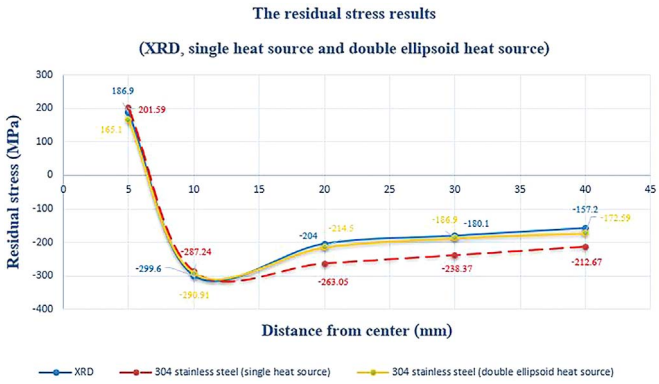

Figure 15. Residual stress in 304 stainless steel determined by XRD, single heat source, and double-ellipsoid heat source.

welds and rapidly cool down during welding. The measured value of FEA of 304 stainless steel (double-ellipsoid heat source) is 165.10 MPa, which the tolerance range measured by XRD is 186.9 ± 20.0 mm (166.9–206.9 MPa). Therefore, the residual stress value is considered consistent, which a difference is 13.20%.

The distance from the center of the weld at 10 mm is near the HAZ. The measured value of FEA of 304 stainless steel (double-ellipsoid heat source) is −290.91 MPa, in which the tolerance range measured by XRD is −299.6 ± 26.1 mm (273.5–325.7 MPa). Therefore, the residual stress value is considered consistent, which a difference is 2.99%.

The distance from the center of the weld at 20, 30, and 40 mm is the area tested. The measured values of FEA of 304 stainless steel (double-ellipsoid heat source) are −214.5, −186.9, and −172.59 MPa, which the tolerance range measured by XRD is −204.0 ± 37.0 mm (167–241 MPa), −180.1 ± 46.1 mm (134–226.2 MPa), and −157.2 ± 55.4 mm (101.8–212.6 MPa), respectively. Therefore, the residual stress values are considered consistent, which a difference is 5.15%, 3.77%, and 9.79%, respectively.

The data obtained from table 6 is analyzed for statistical results, a paired t-test analysis of a hypothetical experiment. The statistical analysis indicated that the acquired p-values (0.148) are greater than 0.05 and 0 inside a 95% confidence interval. Therefore, it can be concluded that both sets of data are no significant differences. By comparing residual stresses, we can be accepted the welding model and confirmed that the value is correct by the FEA method.

From the graph in figure 15, according to the abovementioned criteria, it was determined that the heat of the double-ellipsoid heat source specimen was accurate, and the effect of residual stress was similar to that of the single heat source specimen determined from the actual welding. The measurement of residual stress by XRD was compared to residual stress from the finite element model. Moreover, residual stress in the longitudinal direction was tensile (positive) at a distance of 5 mm from the middle of the weld beads. Residual stress in the longitudinal direction was mostly tensile in the area near the weld beads. This tensile residual stress usually affects fatigue crack initiation in the material.

Table 7. Comparison of longitudinal residual stress results from XRD and FEA of 2024 aluminium alloy.

Distance from the weld center (mm)	0	5	10	20
FEA without porosity (MPa)	−22.730	17.230	−32.319	−24.171
XRD (MPa)	−34.37	70.35	−14.62	−10.00
	±52.10	±10.00	±15.40	±47.30
FEA with porosity (MPa)	−25.044	61.370	−10.44	−12.504

In table 7, The 0 mm is the middle of the welding line with very high temperatures during welding, which is an important area. The measured value from FEA is −25.044 MPa. The tolerance range measured by XRD is −34.37 ± 52.1 mm (17.73–86.47 mm), which has different values equal to 9.3269 MPa.

The distance from the center of the weld at 5 mm is near the welding line, which is the area of the heat-affected zone (HAZ). There is a very high temperature, but the temperature is not high enough to melt into the welds and rapidly cool down during welding. The measured value of FEA is 61.37 MPa. The tolerance range measured by XRD is 70.35 ± 10.0 mm (60.35–80.35 mm), which has different values equal to 8.98 MPa.

The distance from the center of the welds at 10 mm is the area tested. The measured value of FEA is −10.44 MPa. The tolerance range measured by XRD is −14.62 ± 15.4 mm (0.78–30.02 mm), which has different values equal to 4.18 MPa.

The distance from the center of the welds at 20 mm is the area tested. The measured value of FEA is −12.504 MPa. The tolerance range measured by XRD is −10.00 ± 47.3 mm (−37.3–57.3 mm), which has different values equal to 2.504 MPa.

Finite element analysis must account for the presence or absence of porosity within the weld zone of 2024 aluminium alloy. The FEA model simulates only sample number 7 owing to cost constraints. Thus, the most porous sample was selected.

The data obtained from table 7 is analyzed for statistical results, a paired t-test analysis of a hypothetical experiment. The statistical analysis indicated that the acquired p-values (0.911) are greater than 0.05 and 0 inside a 95% confidence interval. Therefore, it can be concluded that both sets of data are no significant differences. By comparing residual stresses, we can be accepted the welding model and confirmed that the value is correct by the FEA method. The schematic of 3D full images was imported to ANSYS software for image analysis and visualization as shown in figure 17.

8. Discussion

8.1. Porosity analysis

Generally, most industries use advanced tools to help detect faults or other defects that occur in the welding process and to reduce inspection time and to obtain quality workpieces or materials for applications such as Radiographic Testing (RT). RT is a radiographic test. Radiographic testing is the method of detecting defects inside the material using radioactive material and the film to record data, most of these methods are used in pipe and welding, etc. The RT [31] method provides preliminary results and shows a virtual 2D of pores. While, the detection of internal porosity is often performed by means of an x-ray method after welding, which is often used off-line. Actually, because of the high cost, only some critical weldments (used in aviation, aerospace, nuclear, etc) require100% inspection by x-ray [8], while most common weldments require merely a spot check. X-ray sources with smaller spot sizes and CT-cone-beam systems with better resolution are the quality of three-dimensional CT will increase. At the same time, our results come from measurements by a three-dimensional x-ray computed tomography (CT or XCT) method. The CT method can measure the size, volume, and volume of all the pores that are better. The pictures of porosities are displayed into three-dimensions, which can convert files and import into the finite element analysis programs more conveniently and easily. Overlapping pores, CT techniques can scan and store data. So, when used CT method in the model, the simulations are more accurate than other techniques.

8.2. Residual stress analysis with the finite element model

The most significant parameters for the prediction of residual stress in the mechanical analysis were the temperature dependence [7] of the yield properties of the plate material. The approach has been validated successfully against direct measurements of the residual stress field made via x-ray diffraction. This is important because there are too many parameters for a systematic parametric experimental study (arc current, welding

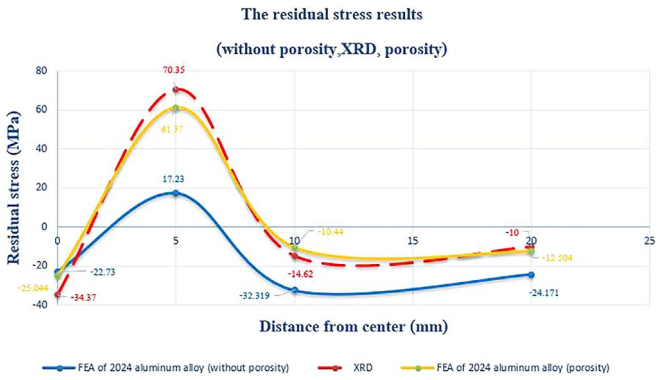

Figure 16. Comparison of residual stress from the without porosity, XRD, and porosity results of 2024 aluminium alloy (3.2 mm thickness).

speed and wire feed rate, the distance ahead of the arc, etc) to be feasible. The non-uniform cooling rate within the materials induced residual stress after 2 specimens were welded together [22]. From these angles, the atomic spacing of the diffracting lattice planes is received by using Bragg's law [44, 46]. Researches, residual stresses were analyzed various methods by curvature measurement [47], hole drilling [48], synchrotron x-ray [49], and magnetic & electrical techniques [11], etc. Positions for measurement by XRD and FEA model were at the following distances from the middle of the welding line such as 0, 5, 10, 20, 30, 40 mm (Transverse direction). The residual stress result by XRD shown in figures 18 and 19, were found that the welding bead zone had compressive residual stresses. The result of residual stress obtained from a non-destructive measurement by the XRD method was compared with the results from the FEA model on a given condition.

A finite element analysis using shell elements has been conducted to model the generation of residual stresses caused by TIG welding of 3.2 mm aluminium alloy 2024 plate. Appropriate selection of heat sink conditions was important to obtain accurate thermal histories [3]. After the FEA was verified, the design of the experiment was firstly used for determining experimental conditions. It was more cost-effective for using data from a verified FEA model than obtained directly from measurements [22]. Therefore, in research the values of residual stresses were obtained from varying main effects conditions in the FEA model, the output results were then analyzed statistically by MINITAB software. The residual stresses from welding simulation by finite element analysis methods were compared with measurements by x-ray diffraction shown in figures 15 and 16.

From graph figure 16, the residual stress obtained from XRD, single heat source, and double-ellipsoid heat source methods at thickness 3 mm. The research of Baisukhan *et al* [44] shown the residual stress results in 304 stainless steel by XRD and FEA (single heat source), in which the residual stress values are consistent and similar. To confirm the correctness of the heating model during the actual welding process and to be realistic as possible for the FEA model, the FEA will compare with two heat sources (single source and double-ellipsoid heat source). After that, we simulate the FEA (double-ellipsoid heat source) model of 304 stainless steel, the residual stress data of FEA (single heat source) of [44] are compared. The double-ellipsoid heat source is closer to the actual welding measured by XRD than the single heat source. The double ellipsoid heat source is a volumetric heat source with a 'Gaussian Distribution Based Double-Ellipsoid Moving Heat Source', which provides more accurate results than a single point or single heat source.

Application of the finite element method in the GTAW process with porosity, there is not much research. Bouafia *et al* [50], used 3D finite element stress in the stress concentration factor of steel welding points (joint) and the porous effect that occurs in the weld nugget process. The porous welding structure is under uniaxial tensile stress using numerical analysis. Meanwhile, Weiler *et al* [51] used the finite element method to predict the high-pressure casting behavior of AM60B magnesium alloy under constant load. Effect of pore sizes and positions by using LS-DYNA software for analysis.

In most cases, the simulation of finite element analysis is found to be neglected in the insertion of pores or other abnormalities. In the case that there are not many porosities, it will be assumed that there are no pores in the model. Given the relatively large number and size of most pores, these small pores probably have no significant role to play in deformation. This research incorporates pores into the simulation which is a new technique. It makes the results more consistent. From graph figure 17, the residual stresses showed from FEA of 2024 aluminium alloy model without porosity (double ellipsoid heat source), XRD results of 2024 aluminium alloy with porosity, and FEA of 2024 aluminium alloy model with porosity (double ellipsoid heat

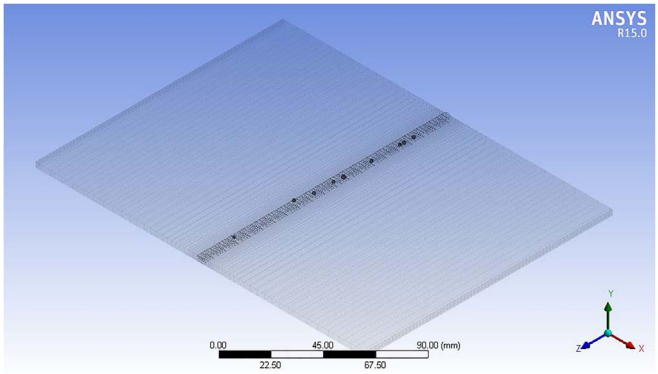

Figure 17. Schematic of 3D full images was imported to ANSYS software for image analysis and visualization.

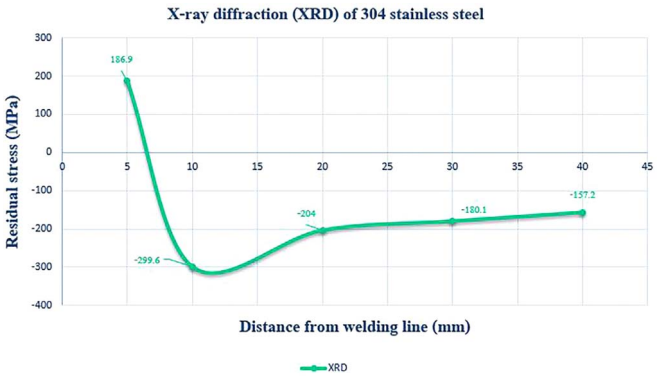

Figure 18. The residual stress result by XRD (304 stainless steel).

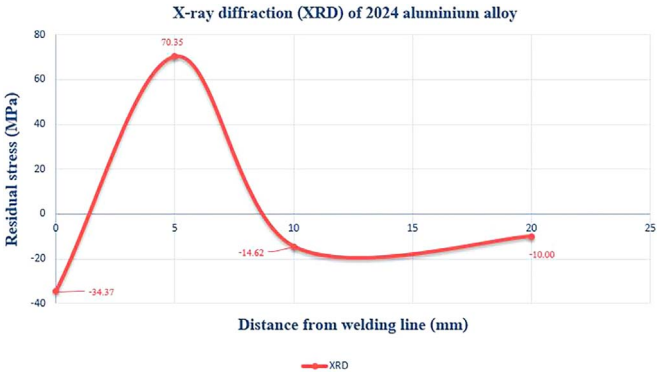

Figure 19. The residual stress result by XRD diffraction (2024 aluminium alloy).

source). From the FEA simulation, it is found that the porous simulation is more than consistent with the actual workpiece. The occurrence of porosity, including the porous distribution that occurs in the welding line, affects the residual stress values of welding workpiece. The FEA simulation can predict without inferior to other methods, but we have additional applications to make the model accurate and consistent. Therefore, it was deduced that the FEA model for computing temperature field and residual stress during welding are valid, and subsequently, this validation leads to the conclusion that we can use the FE model with porosity for predicting the weld.

9. Conclusions

1. The CT analysis showed porosity at the weld area produced at various welding speeds. It was observed that porosity was most prevalent for condition 7 (sample number 7).
2. A more rigorous experiment on the effect of porosity on residual stress can be performed in the future at different positions along the weld zone and at specific locations.
3. This method was compared to the direct measurements of the residual stress field obtained with XRD.
4. The values of residual stress from XRD, single heat source, and double-ellipsoid heat source for the thickness of 3 mm are consistent and similar. It was determined that the double-ellipsoid heat source provided more accurate residual stress results compared to the actual XRD measurement of a single heat source. The double-ellipsoid heat source is a volumetric heat source. It has a 'Gaussian Distribution-Based Double-Ellipsoid Moving Heat Source', which provides more accurate results than a spot heat source, which is also known as the single heat source.
5. The simulations of FEA models containing pores showed that porous models were more similar (residual stress values) to the actual welding results than models without pores.

Acknowledgments

The authors are grateful to the Thailand Graduate Institute of Science and Technology (TGIST) for financial support. The authors are also grateful to the National Metal and Materials Technology Center (MTEC) for financial, machinery and equipment support. The authors are also grateful to the Advanced Manufacturing Technology Research Centre (AMTech), Chiang Mai University for their facility support and financial sponsorship of this research.

ORCID iDs

Pattarawadee Poolperm https://orcid.org/0000-0003-0115-6819

References

[1] Sivashanmugam M, Kumar T, Jothi Shanmugam C and Sathishkumar M 2010 Investigation of microstructure and mechanical properties of GTAW and GMAW joints on AA7075 aluminum alloy *In Frontiers in Automobile and Mechanical Engineering* **197** 241–6 (https://ieeexplore.ieee.org/abstract/document/5714843)
[2] Balasubramanian V, Ravisankar V and Reddy G M 2008 Effect of postweld aging treatment on fatigue behavior of pulsed current welded AA7075 aluminum alloy joints *J. Mater. Eng. Perform.* **17** 224–33
[3] Na Z H A O, Yang Y O, Ming H A N, Xian L U O, Feng G H and Zhang R J 2012 Finite element analysis of pressure on 2024 aluminum alloy created during restricting expansion deformation heat treatment *Transactions of Nonferrous Metals Society of China* **22** 2226–32
[4] Lakshminarayanan A K, Balasubramanian V and Elangovan K 2009 Effect of welding processes on tensile properties of AA6061 aluminium alloy joints *The International Journal of Advanced Manufacturing Technology* **40** 286–96
[5] Varghese V J, Suresh M R and Kumar D S 2013 Recent developments in modeling of heat transfer during TIG welding—a review *The International Journal of Advanced Manufacturing Technology* **64** 749–54
[6] Goeppner G A 1996 TIG welding of aluminum alloys for the APS storage ring-a UHV application *U.S. Department of Energy Office of Scientific and Technical Information* 28 (IL (United States): Argonne National Lab) 1–15 (https://osti.gov/servlets/purl/379062-qEx8Br/webviewable/)
[7] Preston R V, Shercliff H R, Withers P J and Smith S D 2003 Finite element modeling of tungsten inert gas welding of aluminium alloy 2024 *Sci. Technol. Weld. Joining* **8** 10–8
[8] Yu H, Xu Y, Song J, Pu J, Zhao X and Yao G 2015 On-line monitor of hydrogen porosity based on arc spectral information in Al-Mg alloy pulsed gas tungsten arc welding *Optics & Laser Technology* **70** 30–8
[9] Sarkani S, Tritchkov V and Michaelov G 2000 An efficient approach for computing residual stresses in welded joints *Finite Element in Analysis and Design* **35** 247–68
[10] Schajer G S 1988 Measurement of non-uniform residual stresses using the hole-drilling method. Part II—practical application of the integral method *ASME Journal of Engineering Materials and Technology* **110** 344–9
[11] Withers P J and Bhadeshia H K D H 2001 Residual stress. Part 1-measurement techniques *Mater. Sci. Technol.* **17** 355–65
[12] Prevey P S 1986 X-ray diffraction residual stress techniques *ASM International, ASM Handbook* **10** 380–92
[13] Nelson D, Fuchs E, Makino A and Williams D 1994 Residual-stress determination by single-axis holographic interferometry and hole drilling: II. Experiments *Exp. Mech.* **34** 79–88
[14] Preston R V, Shercliff H R, Withers P J, Hughes D J, Smith S D and Webster P J 2006 Synchrotron x-ray measurement and finite element analysis of residual strain in tungsten inert gas welded aluminum alloy 2024 *Metallurgical and Materials Transactions* **37** 3629–37
[15] Ahmadzadeh M, Farshi B, Salimi H R and Fard A H 2013 Residual stresses due to gas arc welding of aluminum alloy joints by numerical simulations *Int. J. Mater. Form.* **6** 233–47

[16] Hong J K, Tsai C L and Dong P 1998 Assessment of numerical procedures for residual stress analysis of multipass welds *Welding Journal-New York* **77** 372–82 (https://app.aws.org/wj/supplement/WJ_1998_09_s372.pdf)
[17] Na S J and Lee S Y 1987 A study on the three-dimensional analysis of the transient temperature distribution in gas tungsten arc welding *Proceedings of the Institution of Mechanical Engineers, Part B: Management and Engineering Manufacture* **201** 149–56
[18] Fricke S, Keim E and Schmidt J 2001 Numerical weld modeling—a method for calculating weld-induced residual stresses *Nucl. Eng. Des.* **206** 139–50
[19] Oddy A S, Goldak J A and McDill J M J 1992 Transformation plasticity and residual stresses in single-pass repair welds *ASME J. Pressure Vessel Technology* **11** 33–8 (https://asmedigitalcollection.asme.org/pressurevesseltech/article-abstract/114/1/33/436453)
[20] Rybicki E F, McGuire P A, Merrick E and Wert J 1982 The effect of pipe thickness on residual stresses due to girth welds 204–9
[21] Zubairuddin M, Albert S K, Mahadevan S, Vasudevan M, Chaudhari V and Suri V K 2014 Experimental and finite element analysis of residual stress and distortion in GTA welding of modified 9Cr-1Mo steel *J. Mech. Sci. Technol.* **28** 5095–105
[22] Baisukhan A, Nakkiew W and Pitjamit S 2015 Design of experiment for predicting residual stresses in gas tungsten arc welding process, In Industrial Engineering *Management Science and Applications* **349** 77–84
[23] Klobčar D, Tušek J and Taljat B 2004 Finite element modeling of GTA weld surfacing applied to hot-work tooling *Comput. Mater. Sci.* **31** 368–78
[24] Wei E, Farson D, Richardson R and Ludewig H 2001 Detection of weld surface porosity by statistical analysis of arc current in gas metal arc welding *J. Manuf. Processes* **3** 50–9
[25] Bakker K, Kwast H and Cordfunke E H P 1995 Determination of a porosity correction factor for the thermal conductivity of irradiated U02 fuel by means of the finite element method *J. Nucl. Mater.* **226** 128–43
[26] Poolperm P and Nakkiew W 2016 Effect of porosity on residual stress of 2024-aluminum GTAW specimen In*Mater. Sci. Forum* **872** 28–32
[27] Kohandehghan A R, Serajzadeh S and Kokabi A H 2010 A study on residual stresses in gas tungsten arc welding of AA5251 *Mater. Manuf. Processes* **25** 1242–50
[28] Azar A S 2015 A heat source model for cold metal transfer (CMT) welding *J. Therm. Anal. Calorim.* **122** 741–6
[29] Kong F and Kovacevic R 2010 3D finite element modeling of the thermally induced residual stress in the hybrid laser/arc welding of lap joint *J. Mater. Process. Technol.* **210** 941–50
[30] Attarha M J and Sattari-Far I 2011 Study on welding temperature distribution in thin welded plates through experimental measurements and finite element simulation *J. Mater. Process. Technol.* **211** 688–94
[31] Deng D 2009 FEM prediction of welding residual stress and distortion in carbon steel considering phase transformation effects *Mater. Des.* **30** 359–66
[32] Slováček M, Diviš V, Junek L and Ochodek V 2005 Numerical simulation of the welding process—distortion and residual stress prediction, heat source model determination *Welding in the World* **49** 15–29
[33] Rotundo F, Morri A and Ceschini L 2012 Linear friction welding of a 2024 Al alloy: microstructural, tensile and fatigue properties *Light Metals* **2012** 493–6
[34] Wang Y and Zhao P 2001 Noncontact acoustic analysis monitoring of plasma arc welding *Int. J. Press. Vessels Pip.* **78** 43–7
[35] Wikle Iii H C, Kottilingam S, Zee R H and Chin B A 2001 Infrared sensing techniques for penetration depth control of the sub-merged arc welding process *J. Mater. Process. Technol.* **113** 228–33
[36] Xu Y, Yu H, Zhong J, Lin T and Chen S 2012 Real-time image capturing and processing of seam and pool during robotic welding process *Industrial Robot: An International Journal* **39** 513–23
[37] Kastner J, Plank B and Requena G 2012 Non-destructive characterisation of polymers and Al-alloys by polychromatic cone-beam phase contrast tomography *Mater. Charact.* **64** 79–87
[38] Ziółkowski G, Chlebus E, Szymczyk P and Kurzac J 2014 Application of x-ray CT method for discontinuity and porosity detection in 316L stainless steel part s produced with SLM technology *Science Direct* **14** 608–14
[39] Jiang L, Chawla N, Pacheco M and Noveski V 2011 Three-dimensional (3D) microstructural characterization and quantification of reflow porosity in Sn-rich alloy/copper joints by x-ray tomography *Mater. Charact.* **62** 970–5
[40] Mousavi S A and Miresmaeili R 2008 Experimental and numerical analyses of residual stress distributions in TIG welding process for 304L stainless steel *J. Mater. Process. Technol.* **208** 383–94
[41] Deng D and Murakawa H 2006 Numerical simulation of temperature field and residual stress in multi-pass welds in stainless steel pipe and comparison with experimental measurements *Comput. Mater. Sci.* **37** 269–77
[42] Owen R A, Preston R V, Withers P J, Shercliff H R and Webster P J 2003 Neutron and synchrotron measurements of residual strain in TIG welded aluminium alloy 2024 *Materials Science and Engineering:* A **346** 159–67
[43] Seto N, Katayama S and Matsunawa A 2001 Porosity formation mechanism and suppression procedure in laser welding of aluminum alloy *Weld. Int.* **15** 191–202
[44] Baisukhan A and Nakkiew W 2015 Finite element analysis of residual stress level prediction for TIG welding process In*Applied Mechanics and Materials* **752** 500–4
[45] Yang Z, Ha S, Jang B S and Lee Y 2018 Effect of welding residual stress redistribution on the Charpy absorbed energy *J. Mech. Sci. Technol.* **32** 4345–56
[46] Anderoglu O 2005 Residual stress measurement using x-ray diffraction *Doctoral dissertation* Texas A&M University
[47] Clyne T W and Gill S C 1996 Residual stresses in thermal spray coatings and their effect on interfacial adhesion: a review of recent work *J. Therm. Spray Technol.* **5** 401
[48] Nelson D V, Makino A and Fuchs E A 1997 The holographic-hole drilling method for residual stress determination *Opt. Lasers Eng.* **27** 3–23
[49] Daniels J E and Drakopoulos M 2009 High-energy x-ray diffraction using the Pixium 4700 flat-panel detector *J. Synchrotron Radiat.* **16** 463–8
[50] Bouafia F, Boualem S, El Amin M M and Benali B 2011 3D finite element analysis of stress concentration factor in spot-welded joints of steel: the effect of process-induced porosity *Comput. Mater. Sci.* **50** 1450–9
[51] Weiler J P and Wood J T 2009 Modeling fracture properties in a die-cast AM60B magnesium alloy: II. The effects of the size and location of porosity determined using finite element simulations *Materials Science and Engineering:* A **527** 32–7